

Estimating the age-dependent physical parameters of kiwifruit with non-contact acoustic measurements

Laura A. Cobus^{1,*} and Kasper van Wijk¹

¹*Dodd-Walls Centre for Photonic and Quantum Technologies, New Zealand and Department of Physics,
University of Auckland, Private Bag 92109, Auckland, New Zealand*

(Dated: March 14, 2022)

We present non-contact acoustic measurements of the mechanical properties of a golden kiwifruit. With a laser source in emission, we measure the transmitted acoustic waves using a rotating laser ultrasound detector with a fibre head. Two main propagating waves are observed; a low-frequency Rayleigh wave, and a high frequency wave which propagates through the outer flesh of the fruit. Theoretical modeling of this second wave enables estimates of the wave velocity in the two outer layers of the fruit flesh, and of several viscoelastic parameters. In particular, we find that both acoustic wave velocities, Young's modulus E , and bulk modulus K evolve with fruit age, while the high-frequency wave velocity and K also differ between outer and inner fruit layers.

INTRODUCTION

Non-destructive evaluation of the internal structure of fruit is important for industrial quality assurance and monitoring. Traditionally, the most common parameter used to quantify overall fruit ripeness has been *firmness* – the force required to deform fruit flesh [1]. Firmness is an extensive parameter (dependent on fruit size and shape), but is related Young's modulus E [2, 3] – a spatially-averaged intensive viscoelastic parameter of the fruit flesh. To measure this and other viscoelastic parameters, acoustic-based methods are a natural choice, as acoustic wave propagation is directly related to the mechanical properties of the medium.

One of the most popular acoustic approaches to date is acoustic resonance spectroscopy, in which vibrations in the fruit are induced by impact with a small hammer or by a vibrating table, and the resulting modal spectrum is measured with a microphone or Laser Doppler Vibrometer (LDV). It is now well-established that features of this spectrum correlate with the overall fruit firmness [4]; in addition, this type of measurement can be used to estimate a range of viscoelastic parameters [5–9], each giving slightly different information on fruit flesh properties. Acoustic velocity (measured in the temporal domain) has also been shown to correlate with fruit age and/or firmness [9–16]. It remains, however, an ongoing research question as to which parameter may be the most relevant in terms of fruit quality monitoring. The answer may be different for different types of fruit. The quality of fruit may also be strongly affected by its inner structure, motivating research into the properties of individual fruit layers. The majority of such work is destructive, requiring the examination of sections of extracted fruit flesh [17–23] or carried out by pushing a probe through the fruit [24]. However, a few recent studies have exploited the sensitivity of acoustic waves to density variations in the propagation medium for non-destructive evaluation of different flesh layers. A few groups have used acoustic waves propagating on the fruit surface to estimate the properties of the outer flesh layer [14, 16], and Yoshida et al. have employed Doppler ultrasound imaging in fruit to reveal its inner structure [25]. These studies show that, while vibrational methods are effective for determining some properties of the fruit as a whole, and to signal the presence of defects [26–28], acoustic measurements in the temporal domain may have more potential to examine the inner structure of fruit in detail.

In this context, we have developed a temporal acoustic approach for the characterization of kiwifruit. Kiwifruit are the most valuable export in New Zealand [29]; however, detailed measurements of their mechanical properties are rare. Parameters which correlate with overall kiwifruit firmness have been measured using acoustic resonance methods with an LDV in detection and with a non-contact electronic waveguide [30]. However, kiwifruit are heterogeneous, consisting of a thin outer skin, and three inner fleshy layers: the outer pericarp, inner pericarp, and core [31] (Fig. 1A). Using a penetrometer, Jackson et al. found that the core is the most firm, while the inner pericarp is the least firm, most likely because it has a higher liquid content with seed inclusions [24]. More recently, Kenpeng et al. and Du et al. carried out compression testing on extracted portions of kiwifruit flesh to estimate Young's modulus [21, 22] in the outer pericarp and core. To our knowledge, these studies – all of which use destructive testing methods – have been the only attempts to differentiate between kiwifruit layers.

Here, we present entirely non-contact and non-destructive measurements of a variety of viscoelastic parameters in kiwifruit flesh layers. We record the time- and position- dependent transmitted acoustic waves through a golden kiwifruit (*Actinidia chinensis*). As the fruit ages, we record multiple sets of these measurements. Previous measurements of viscoelastic parameters on fruit show that some, or all, should correlate directly with firmness, and thus

should offer a way to monitor fruit age/quality [9, 17, 32]. However, such studies are few and far between, and it is not clear which parameter might be the best for monitoring fruit quality. In a previous study on apples, we found a remarkable similarity between these datasets and those measured in seismology. We thus used a seismology-inspired methodology to analyze the data, showing that a range of viscoelastic parameters can be estimated [9]. Here, we apply a similar approach to kiwifruit. We find that more detailed and higher quality data offer insights into the more complex inner structure of kiwifruit. We present an analysis of such a dataset, acquired using a single fruit; as such, this work is not meant to be representative of a large sample of kiwifruit, but rather to be an initial proof-of-concept experiment. The aims here are to investigate how to interpret these experimental datasets, to determine whether an analysis based on an assumption of homogeneity can be applied to the kiwifruit studied here, and to investigate the potential of this approach for estimating age-related changes in individual kiwifruit layers. In particular, it is of interest to determine which experimental observables correlate with physical changes caused by ageing in the fruit flesh.

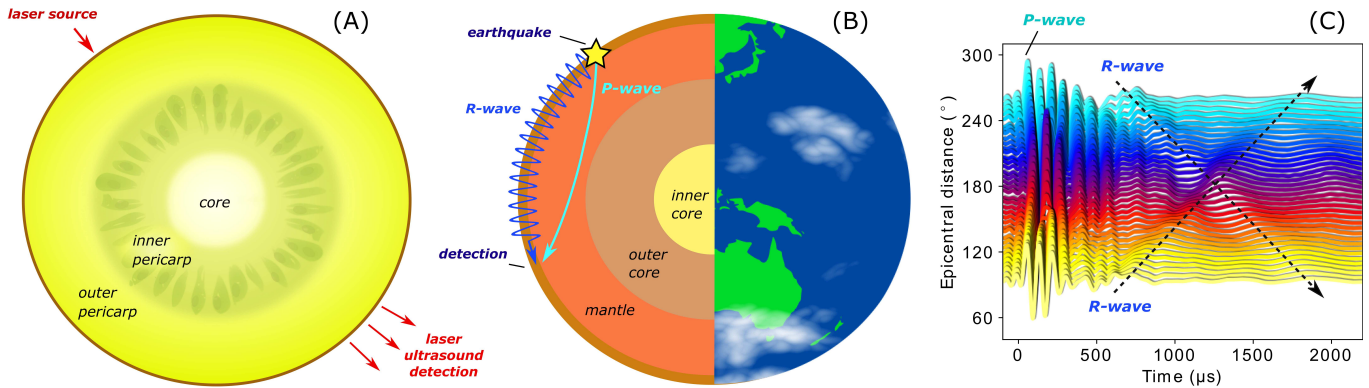


FIG. 1. Graphical representation of the analogy between (A) acoustic propagation through the three layers of a kiwifruit, and (B) seismic wave propagation through the three layers of the Earth. (C) Wiggle plot of angle- and time-dependent transmitted acoustic waves through a kiwifruit. At first glance, P- and R-waves appear to be easily identifiable.

MATERIAL AND METHODS

Experiment

In our measurements, a high-powered pulsed laser is aimed at one side of the kiwifruit to excite an acoustic waveform in the fruit via non-destructive thermoelastic expansion. On the opposite side of the kiwifruit, a Laser Doppler Vibrometer (LDV) measures any displacement of the surface of the fruit. The LDV is rotated around the equator of the kiwifruit to measure the surface displacement at points around the fruit (Fig. 1A). To observe age/ripeness-related changes in the fruit, these measurements were repeated multiple times over a time period of 74 hours.

The source used to create elastic waves was a Quanta-Ray INDI pulsed laser (central wavelength 1064 nm, pulse energy 270 mJ, pulse duration 10 ns, beam diameter 4 mm, repetition rate 10 Hz). The LDV detector was a Polytech OFV-5000Xtra and a MLV-I-120 sensor head, with a flexible fibre optic cable and lens attached. The detection beam could be focused through the cable and lens to a point of 3 mm on the fruit surface. Reflective tape was applied around the fruit equator to optimize the amount of detected light. Signals were recorded by an Alazar Tech digital oscilloscope card at 1 MS/s and 16-bits dynamic range. The entire data acquisition system was controlled by the open-source software PLACE [33]. We have previously reported the approach described above to study apples [9], with the exception of the detection sensor head which was placed on a long rotating arm. Now, with the sensor head attached to a fibre optic cable, the data collection is much more flexible, reliable and rapid.

The golden kiwifruit studied was purchased from a local grocery store. Data was recorded at seven different times spanning a time lapse of 74 hours, beginning with the day the fruit was purchased. For each data acquisition, the fibre head was rotated around the fruit from $\theta \approx 90^\circ - 280^\circ$, stopping at intervals of 10° to record the transmitted time-dependent longitudinal waves. Between acquisitions the fruit was left to sit in the same spot. Fruit volume was measured using Archimedes' principle; both volume and weight were measured before and after the entire time lapse,

and extrapolated values were calculated for the other acquisition times, assuming a linear rate of change between first and last points. From these points, density ρ was estimated.

Analysis and interpretation

Using the approach described previously, each dataset acquired is a matrix of transmitted acoustic signals $R(\theta, t)$, where t is the time recorded after the source excitation, and *epicentral distance* θ is the angle between source and detector points. This type of dataset is directly analogous to that acquired in seismology, in which multiple detectors on the surface of the Earth detect vibrations resulting from far-off seismic events (Fig. 1B). Figure 1C shows a representative example of $R(\theta, t)$. Referred to as a *wiggle plot* in seismology, this type of figure facilitates distinction between the different types of waves which contribute to the total transmitted wavefield. In Fig. 1C, two different waves can be seen by eye. In seismology, these waves would be interpreted as (i) a direct compressional wave, called the ‘P-wave’ in seismology, and (ii) surface Rayleigh waves travelling around each side of the fruit, called the ‘R-wave’. For each wave, of interest is the time at which the wave arrives at each detector position. These *arrival times* were determined using the following steps: (i) first-arriving signals were identified by eye for traces recorded at $\theta = 180^\circ$, (ii) temporal cross-correlation of signals recorded at different source-detector angles was used to determine the relative arrival times for the range of detector positions, and (iii) these times were corrected by the first arrival time at $\theta = 180^\circ$. This process was performed for both the P- and R-waves.

Estimating acoustic wave velocity

R-wave velocity v_R can be measured by performing a linear fit of the arrival time t_R of the transmitted signal versus the distance travelled around the fruit surface, d_{surface} [9, 15]. However, care must be taken, as near $\theta = 180^\circ$ the data contains a superposition of the two R-waves that have travelled around the epicenter of the fruit in opposite directions – an effect that can be seen by eye in Fig. 1C. This impedes an accurate measurement of R-wave arrival time near $\theta = 180^\circ$. To estimate of v_R , therefore, these points are excluded from the linear fit.

If the fruit is homogeneous, i.e. if acoustic wave velocity is constant throughout the fruit, then the same approach can be taken for P-waves; arrival time t_P should scale linearly with direct distance d_{direct} through the fruit, and P-wave velocity can be found by fitting the data with a linear fit: $v_P = \Delta d_{\text{direct}} / \Delta t_P$. However, the heterogeneous nature of kiwifruit (e.g. Fig. 1B) means that this linear relationship might not always be obeyed. To model P-wave propagation through a heterogeneous fruit, we used software originally designed for seismological ray-racing [34] to simulate compressional wave propagation through a fruit with different layers of flesh. Specifically, we performed this theoretical modeling using the TauP Toolkit [34]. A guess for the depth-dependent velocity profile is defined, and the toolkit estimates the resulting arrival times at points along the surface. By comparing these theoretical predictions with experimental measurements, the velocity model can be optimized, meaning that in principle, an estimate can be obtained of v_P for each layer of the kiwifruit. For this study, we performed this optimization manually.

Estimating other viscoelastic parameters

If both v_R and v_P are known, a range of viscoelastic parameters can be estimated for the kiwifruit. While the experimental setup used here can not detect shear waves (S-waves) directly (as the LDV only measures the longitudinal component of the kiwifruit surface displacement), shear-wave velocity v_S can be estimated from v_R and v_P by finding the real roots of

$$\left(2 - \frac{v_R^2}{v_S^2}\right)^2 + 4\sqrt{\frac{v_R^2}{v_S^2} - 1}\sqrt{\frac{v_R^2}{v_P^2} - 1} = 0, \quad (1)$$

and requiring that $0 < v_R < v_S$. Elastic moduli can then be calculated [35]:

$$E = v_S^2 \rho (2\nu + 2), \quad (2)$$

$$G = E / [2(1 + \nu)], \text{ and} \quad (3)$$

$$K = E / [3(1 - 2\nu)], \quad (4)$$

where E is Young's modulus, G is the shear modulus, K is the bulk modulus, and

$$\nu \equiv \frac{1}{2} \frac{(v_P^2/v_S^2) - 2}{(v_P^2/v_S^2) - 1} \quad (5)$$

is Poisson's ratio. The elastic moduli measure the response of the material to applied deformation: Poisson's ratio quantifies the deformation of a material perpendicular to the direction of an applied force, Young's modulus is the ratio of stress to strain, and thus measures the stiffness of the material, the shear modulus measures the material stiffness with respect to *shear* deformation, and the bulk modulus is related to the inverse of compressibility, representing the change in volume to external stress.

RESULTS AND DISCUSSION

Figure 2 shows transmitted wavefields through a kiwifruit at epicentral distance $\theta = 180^\circ$, measured at seven different time lapses over a 74-hour period. By eye, it seems clear that the first-arriving signal ($t \sim 50 - 250 \mu\text{s}$) corresponds to the P-wave, travelling directly through the fruit flesh, while the later-arriving wave ($t \sim 1000 - 1300 \mu\text{s}$) is the surface R-wave. It can be seen that as the fruit ages, both waves arrive later in time. The frequency content

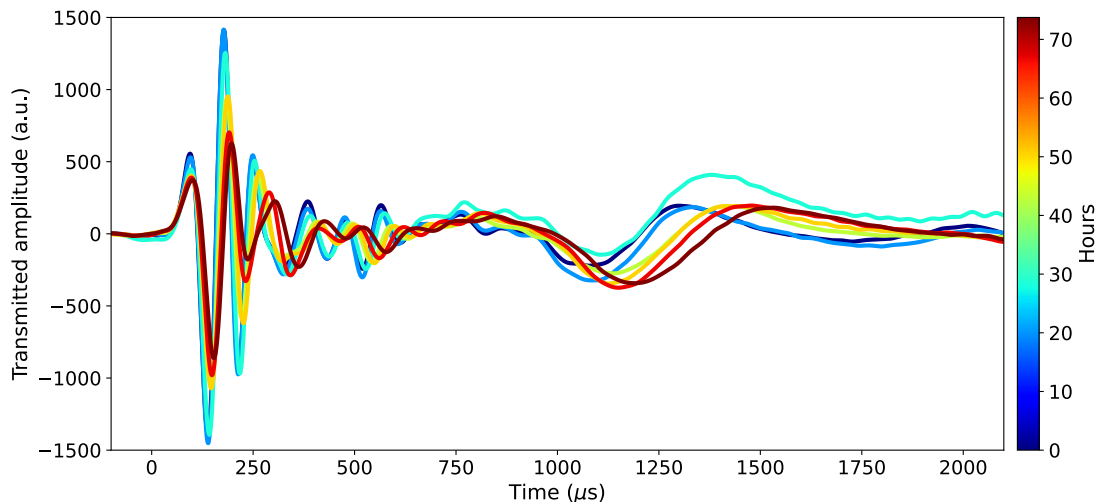


FIG. 2. Transmitted acoustic waves through a golden kiwifruit at $\theta = 180^\circ$, measured periodically over a range of 74 hours.

of these waves also differs; the early-arriving waves are in the range $f = [5 - 16]$ kHz while later arrivals are in the lower range $f = [1 - 4]$ kHz. This means that frequency filtering can be used to isolate each wave from the recorded dataset.

Figure 3 shows a representative example of how the R-wave velocity, v_R , is estimated via a linear fit of distance travelled along the surface, d_{surface} , versus arrival time t . As discussed previously, points near $\theta = 180^\circ$ contain a superposition of two R-waves, and are not included in the linear fit. In Fig. 3, arrival times from waves circling the fruit in both directions (see Fig. 1C) are shown, causing the points to appear to overlap.

Measurement of the velocity of the higher-frequency wave is less straightforward. Figure 4A shows experimentally-measured arrival times for the P-wave at a time lapse of 0 hours, plotted as a function of distance travelled along the surface. A linear fit to the P-wave arrival times $v_P = \Delta d_{\text{direct}} / \Delta t_P$ only just fits the data within the margin of error (Fig. 5A). This observation is similar to that seen in a study by Arai et al., in which two waves propagate in mango flesh at different speeds, both with a roughly linear relationship between angle and arrival time [16]. The interpretation given is that both are surface waves, where one is confined to the skin, the other to the outer flesh layer, and with $v_{\text{skin}} \sim 10v_{\text{flesh}}$. This idea is convincing due to the presence of the hard pit which makes the detection of a bulk compressional wave unlikely. In this case, a simple linear fit of d_{surface} vs t should give the velocity of this surface wave. Figure 4A shows that our data can be described by this simple model. Results for the velocity extracted from the linear fitting are shown in Figure 4B over the entire time lapse period. As observed with v_R , the velocity of this high-frequency wave decreases with fruit age.

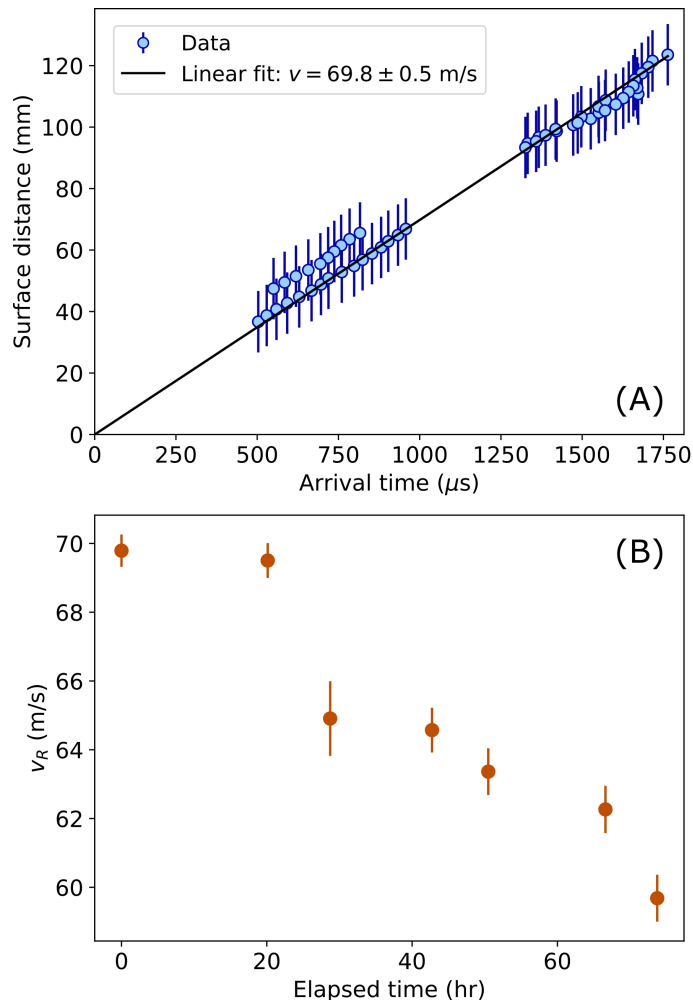


FIG. 3. (A) Experimentally-measured R-wave arrival times are plotted versus d_{surface} , distance travelled along the fruit surface from the source point (symbols). The slope of a linear fit (black line) gives an estimate of velocity v_R . Experimental data shown was measured after a time-lapse of 0 hours. (B) Results for v_R are shown for the entire time lapse period.

An alternative interpretation for the arrival times of the faster coherent wave in Fig. 5A is that the first-arriving wave could also be a compressional P-wave whose propagation is influenced by the heterogeneity of the kiwifruit. In a numerical study on acoustic wave propagation in orange peels, Jimenez et al. also observe a first-arriving wave with a linear relationship between angle and arrival time, but (in contrast with the example of Arai et al. above) interpret this as a (compressional) P-wave [36]. This is equally possible in our case. The argument for a bulk wave is the perceived bias in the linear fit: for short distances, the mean estimated travel time is consistently later than the fit. For large distance, the mean estimated travel time is consistently earlier than the best fit linear model. To investigate this possibility, we now extend our analysis to consider a more realistic fruit model. Figure 5B shows a simplistic, but realistic velocity model for a heterogeneous kiwifruit. The three main layers are represented (Fig. 1A): the outer pericarp (depth $\sim 0 - 12$ mm), with a velocity gradient to the inner pericarp (depth $\sim 12 - 23$ mm), and the smaller core (depth $\sim 23 - 26$ mm). The general form of this model resembles results from experimental measurements by Jackson et al. of depth-dependent firmness in other types of kiwifruit [24]. Here, however, we do not include the skin in our model, as the range of wavelengths of our measurements are likely too large to be sensitive to such a thin layer.

To compare our model with experimental measurements, we simulate the propagation of P-waves through the model using a ray-tracing method which was initially developed to model elastic wave propagation in the Earth. Representative results are shown in Fig. 5. For most source-detector angles, the theoretically-predicted arrival times agree with experimental measurements (Fig. 5A). It is of note that the data is not symmetric about $\theta = 180^\circ$; this is likely due to a slight asymmetry in the fruit shape, and also observed in the R-wave arrival times. The theoretical simulation also gives the paths that the compressional waves take through the velocity model. Figure 5C shows the

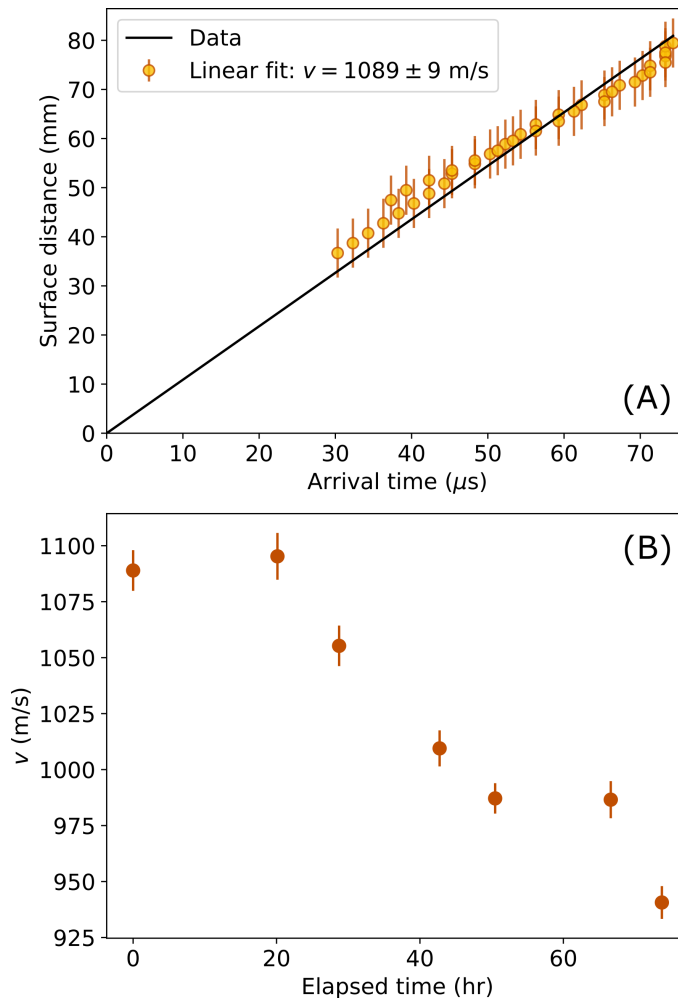


FIG. 4. (A) Experimentally-measured arrival times of the first-arriving wave are plotted versus d_{surface} , distance travelled along the fruit surface from the source point (symbols). Supposing that this wave is a surface wave, the slope of a linear fit (black line) gives an estimate of velocity v . Experimental data shown was measured after a time-lapse of 0 hours. (B) Results for v are shown for the entire time lapse period.

ray paths associated with the simulated arrival times of Fig. 5A. For this velocity model, the P-waves which arrive first to most detectors are those which have travelled around the outer pericarp and the gradient layer between the outer and inner pericarp.

Each of the 7 datasets recorded within the 74-hour time-lapse period show the same approximate scaling of arrival time with distance seen in Fig. 5A. Thus, the ray-tracing simulation and comparison to data was performed for each dataset. In this way, estimates for v_P were obtained for the outer two layers. It is important to note that a very wide variety of velocity models were tested, and none predicted arrival times which agree with the experimental data except those reported here (e.g. Fig. 5B). Results for v_P are shown in Fig. 5D. Changing the core velocity does not impact the simulation results, but a specific – negative – velocity gradient is required between the outer and inner pericarp. Thus, we can estimate v_P in the outer pericarp, and set an upper bound on v_P for the inner pericarp.

Theoretical modeling of compressional wave propagation through a layered fruit shows that the experimentally-measured arrival times correspond to the situation in which P-waves are confined to the outer part of the outer pericarp, near the kiwifruit surface (Fig. 5C). The best-fitting model predicts that the average P-wave speed in the outer pericarp (for a time lapse of 0 hours) is $v_P \sim 945$ m/s. This result is similar to $v = 1089 \pm 9$ m/s – the velocity obtained by interpreting the first-arriving wave as a high-frequency surface wave (Fig. 4B). However, while this approach gives one estimate of acoustic velocity near the fruit surface, the P-wave modeling allows limits to be set for v_P in both the inner and outer pericarp, and for the velocity gradient between them (Fig. 5D). This approach could lead the way to further non-destructive characterization of the kiwifruit inner structure. As we have shown, it

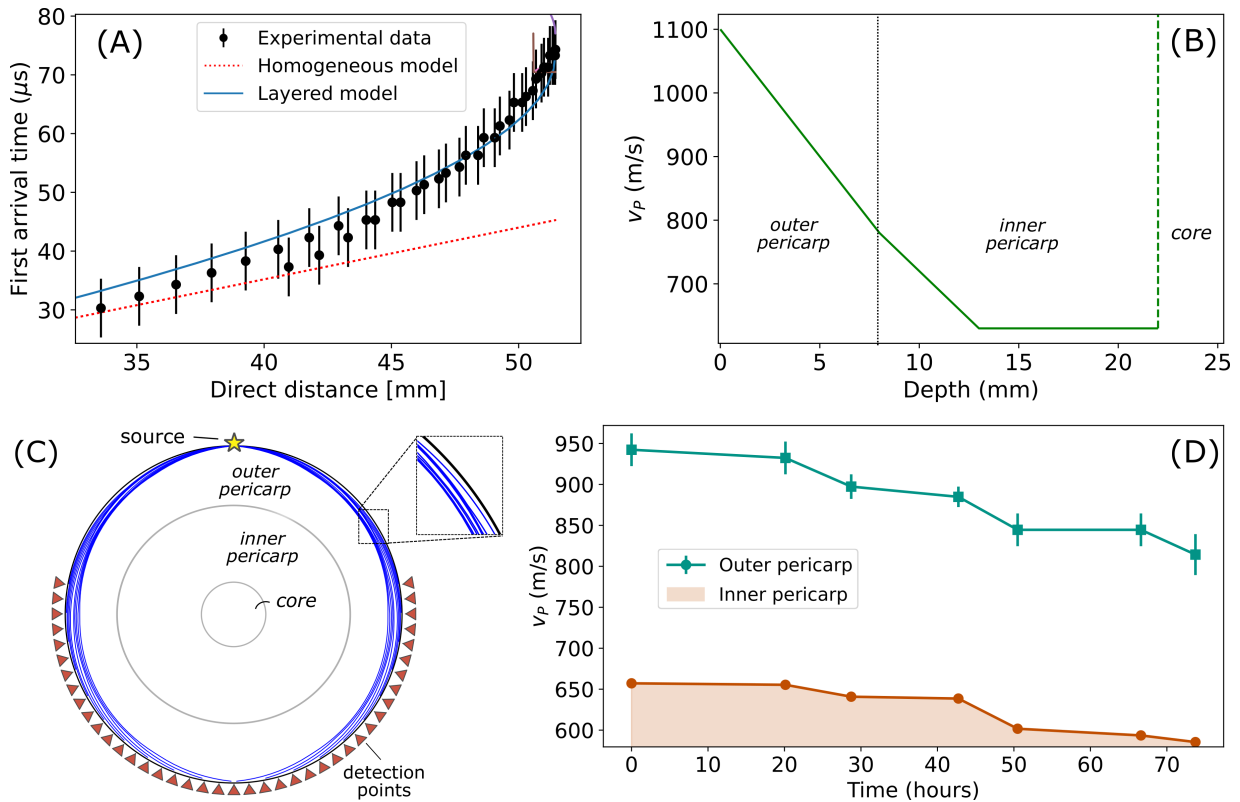


FIG. 5. (A,B) Experimental P-wave arrival times t_P (symbols), acquired at a time lapse of 0 hours, are compared with theoretical predictions from homogeneous (red dotted line) and layered models (green solid lines). t_P is plotted versus (A) d_{direct} (to emphasise the deviation from the homogeneous model). (B) The layered velocity model used to predict t_P in (A,B). Values in the core (depth > 23 mm) do not impact the predictions, and are indicated with a dashed line. (C) Ray paths (blue lines) corresponding to the first-arriving P-wave for the layered model. A zoom of the top right corner shows the individual paths of each ray. (D) Estimates of v_P from comparing experimental and theoretical t_P in the outer pericarp (teal circular symbols) and inner pericarp (orange square symbols), performed for each time-lapse measurement. The shaded orange area indicates that the data points constitute an upper bound for v_P in the inner pericarp.

also allows viscoelastic parameters to be estimated.

With knowledge of v_R , v_P , and density ρ , values for v_S , ν , E , G , and K were calculated for the outer and inner pericarp (Eqns. 1-5). Over the time lapse period, density increased very slightly from $\rho = 1.027 \pm 0.005$ g/cm³ to $\rho = 1.040 \pm 0.005$ g/cm³. The relative long wavelength of the Rayleigh wave velocity v_R compared with the kiwifruit size means that the R-wave likely samples both inner and outer pericarps and the core, with v_R being the average velocity of these layers. Thus, the same v_R value is used in Eq. 1 for both pericarp layers. Results for selected elastic parameters are shown in Fig. 6. We find that while estimates of E and G do not vary significantly between the inner and outer pericarp, they do exhibit a clear decay with fruit age (Fig. 6A,B). Conversely, while ν varies with layer, it does not evolve with fruit age (Fig. 6B). The bulk modulus K is the only elastic parameter to change with both time and spatial location in the fruit (Fig. 6C).

Young's modulus E may be the closest parameter to that which is evaluated by the customer who squeezes a fruit to assess its quality. To our knowledge, E is the only viscoelastic parameter previously measured for kiwifruit; for green kiwifruit (*Actinidia deliciosa*), $E \sim 1 - 5$ MPa [21, 37] and for red-fleshed gold kiwifruit (*Actinidia chinensis* cv. Hongyang), E varied from $E = 2.389 \pm 0.545$ MPa to $E = 0.288 \pm 0.064$ MPa, measured six days later [22]. This decrease of E with fruit age agrees with our observations (Fig. 6B). Our values of $E \sim 9 - 12$ MPa are of the same order of magnitude as the previous values, but consistently larger.

For other types of fruit, a very wide range of values of viscoelastic parameters have been reported. Shockwave-induced Rayleigh waves have been used to measure $v_R \sim 25 - 50$ m/s in the outer flesh of mangos, finding that v_R decreases as the mango ripens [16]. We also observe this trend for kiwifruit ageing, indicating that v_R could be a useful observable for predicting overall kiwifruit age/ripeness. Note that our results for v_R are not shown here, but are proportional to E as shown in Fig. 6A). Our measured values for v_P are slightly higher than those reported for

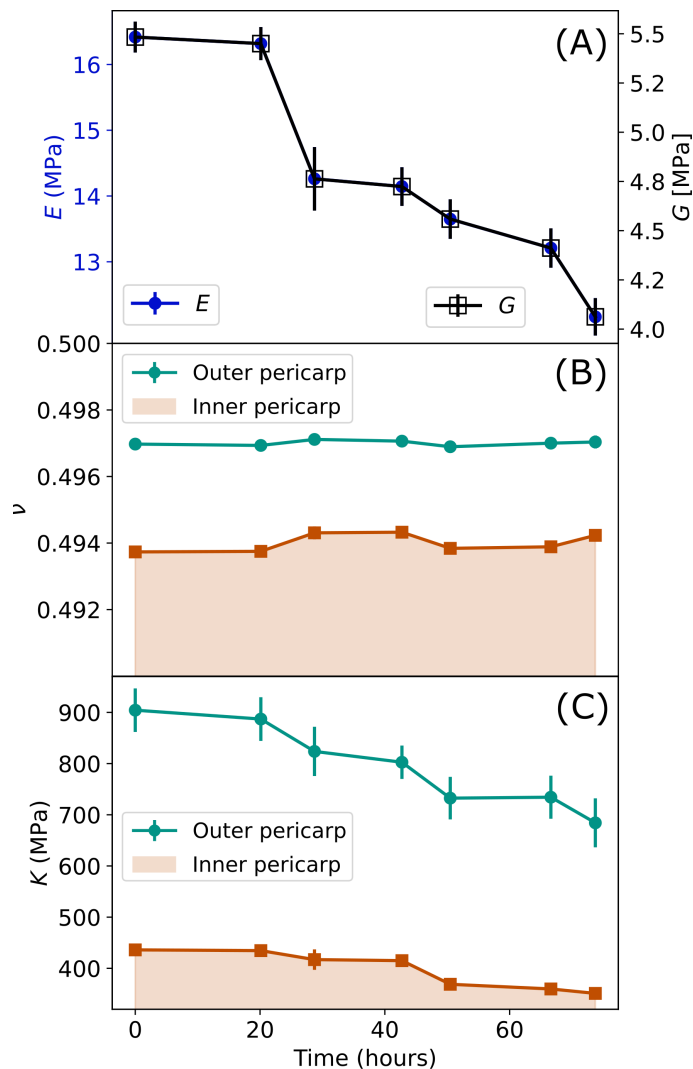


FIG. 6. Elastic wave parameters of a golden kiwifruit, measured over a time period of 74 hours. In (A) E and G in the outer pericarp are shown (values in the inner pericarp are identical, but constitute upper bounds). Values for (B) ν and (C) K are shown for the outer pericarp (teal circular symbols) and inner pericarp (orange square symbols).

apple flesh, melons and avocados ($\sim 100 - 400$ m/s) [9, 18, 38], and are in fact closer those measured for potatoes ($v \sim 500 - 800$ m/s) [39].

Results for the shear modulus G in the outer pericarp are shown in Fig. 6A – values for the inner pericarp are almost identical, but constitute an upper bound. We find that over the time lapse period, $G \sim 3 - 4$ MPa. These values are on the order of estimates for other fruit: $G < 1$ MPa for pomegranates [19] and for banana and apple flesh [23] and $G \sim 5 - 6$ MPa for pear flesh [17]. For Poisson's ratio, $\nu \sim 0.16 - 0.24$ for apples [9], $\nu \sim 0.03 - 0.4$ for apple flesh [17, 23], $\nu \sim 0.408$ for banana flesh [23], and $\nu \sim 0.25 - 0.4$ for pear flesh [17]. We find relatively high values, $\nu > 0.49$ for kiwifruit.

Very few reports of experimental measurements of K for fruit are available: $K \sim 0.4 - 0.8$ MPa has been reported for banana flesh [23], $K \sim 1.5 - 3.1$ MPa for apple flesh [23], and $K \sim 3 - 7$ MPa for peaches [40]. Our values of 200 – 900 MPa for golden kiwifruit are much larger.

There are several possible reasons for the fact that our values of E , K and ν are larger than might be expected. For E , kiwifruit previously studied were of a different type. The kiwifruit studied here was also very firm when measurements began (as evaluated by feel), and was thus perhaps less compressible than other fruit studied. It also possible that cold storage of the fruit before it reached the grocery store increases its compressibility [41]. In general,

however, we can expect elastic constants measured via acoustic techniques to be higher than those using quasi-static stress/strain tests. This effect has been observed for apples [9, 17, 42], orange peel [36] and watermelons [14]. Acoustic methods measure the ‘dynamic’ Young’s modulus E_d , which is similar to the true E , while stress/strain-type approaches measure the ‘apparent’ Young’s modulus E_a , which can be lower than E_d , especially if the material being tested becomes close to deformation. These differences are due to the frequency dependence of the viscoelastic fruit. The loss of information inherent in low-frequency static measurements means that parameters which are sensitive to v_P , a higher-frequency wave, could be underestimated [36]. In addition, acoustic measurements examine the properties of a fruit whose microstructure is unchanged during the experiment, as opposed to deformation experiments which may be closer to examining nonlinear behaviour of the flesh. If the fruit microstructure is even slightly crushed, the value of ν should decrease, with a related change in the other viscoelastic parameters as well. It is possible that fruit with higher water content are more likely to exhibit this effect, having higher values for (high-frequency) bulk compressional waves, most likely a larger difference between v_R and v_P , and a larger resulting value of ν . In that case, parameters such as K which are more sensitive to changes in ν (as opposed to the relatively weak dependence of E on ν) would differ even more drastically from those estimated by low-frequency or quasi-static measurements.

Finally, we note that for the proof-of-concept experiment described here, high source laser power was used in order to optimize signal to noise for easier distinction between P- and R-waves. Over time, this could potentially result in some damage to the fruit at the source point. Future experiments will investigate the lower limits for source power, or employ alternate methods of non-contact excitation which remove the possibility of ablation [16, 43].

CONCLUSION

In conclusion, we have reported the first dynamic measurements of kiwifruit mechanical properties. Using an entirely non-contact experimental approach, we measured different types of waves propagating in the fruit. We are able to observe a deviation from the expected behaviour of the first-arriving wave. Using theoretical modeling inspired by seismological techniques, we find that the first-arriving wave can be interpreted as a compressional wave which is confined to the outermost part of the kiwifruit flesh. This analysis enables us to estimate several viscoelastic parameters for the outer pericarp, and limits on these parameters for the inner pericarp. Considering previous static or frequency-limited measurements for kiwifruit, we observe comparable but slightly higher values of E . We also present the first estimates of K for kiwifruit, which we find to be much higher than those estimated for different types of fruit. These differences could be attributed to the different physical properties measured using dynamic as opposed to static measurements. Finally, we find that many of the viscoelastic parameters estimated are sensitive to fruit age. The simplest observable with which to track kiwifruit ripening is v_R , the velocity of the low-frequency surface wave. However, a more detailed examination of the higher-frequency wave seems promising for probing the fruit’s inner structure.

Future perspectives include analysis of the attenuation of each type of wave, and of the frequency-dependence of acoustic velocities and viscoelastic parameters as the fruit ages. Both of these approaches could give added information and precision in tracking fruit quality. Experimental trials of the presented measurements will be carried out on multiple fruit for a better estimate of typical viscoelastic parameters for golden kiwifruit. Additional accuracy for the modeling of acoustic propagation through a layered kiwifruit could be achieved via comprehensive fitting of the data with a set of theoretical predictions, calculated over the entire space of possible velocities and layer boundary positions.

* laura.cobus@auckland.ac.nz

- [1] J. R. Magness and G. E. Taylor, *Improved type of pressure tester for the determination of fruit maturity*, Tech. Rep. 350 (United States Department of Agriculture, Washington, D.C., 1925).
- [2] R. Lu and J. Abbott, *J. Texture Stud.* **27**, 265 (1996).
- [3] H. Chen and J. DeBaerdemaeker, *J. Agric. Eng. Res.* **56**, 253 (1993).
- [4] W. Zhang, Z. Lv, and S. Xiong, *Crit. Rev. Food Sci. Nutr.* **58**, 2386 (2018).
- [5] S. Falk, C. H. Hertz, and H. J. Virgin, *Physiol. Plant.* **11**, 802 (1958).
- [6] I. J. Davie, N. H. Banks, P. B. Jeffery, C. J. Studman, and P. Kay, *New Zealand Journal of Crop and Horticultural Science* **24**, 151 (1996).
- [7] F. Duprat, M. Grotte, E. Pietri, and D. Loonis, *J. Agric. Eng. Res* **66**, 251 (1997).
- [8] M. Taniwaki, M. Takahashi, and N. Sakurai, *Food Research International* **42**, 137 (2009).
- [9] S. Hitchman, K. van Wijk, and Z. Davidson, *Postharvest Biol. Technol.* **121**, 71 (2016).

- [10] G. K. Self, E. Ordozgoiti, M. J. Povey, and H. Wainwright, *Postharvest Biol. Technol.* **4**, 111 (1994).
- [11] H. Chen, F. Duprat, M. Grotte, D. Loonis, and E. Pietri, *Journal of Texture Studies* **27**, 123 (1996).
- [12] J. Sugiyama, T. Katsurai, J. Hong, H. Koyama, and K. Mikuriya, *Transactions of the ASAE* **41**, 121 (1998).
- [13] E. Macrelli, A. Romani, R. P. Paganelli, E. Sangiorgi, and M. Tartagni, *Sensors and Actuators, A: Physical* **201**, 487 (2013).
- [14] T. Ikeda, P.-K. Choi, T. Ishii, I. Arai, and M. Osawa, *J. Food Eng.* **160**, 28 (2015).
- [15] L. Cobus, J. Simpson, S. Hitchman, J. Shepherd, and K. Wijk, in *Forum Acusticum* (Lyon, France, 2020) pp. 51–54.
- [16] N. Arai, M. Miyake, K. Yamamoto, I. Kajiwara, and N. Hosoya, *Foods* **10**, 323 (2021).
- [17] E. E. Finney, *J. Ag. Eng. Research* **12**, 249 (1967).
- [18] A. Mizrach, N. Galili, and G. Rosenhouse, *Transactions of the American Society of Agricultural Engineers* **32**, 2053 (1989).
- [19] N. Ekrami-Rad, J. K., and M. H. K., *International Journal of Food Properties* **14**, 570 (2011).
- [20] Z. Li, P. Li, H. Yang, J. Liu, and Y. Xu, *Journal of Food Engineering* **111**, 82 (2012).
- [21] T. Kunpeng, S. Cheng, L. Xianwang, H. Jicheng, C. Qiaomin, and Z. Bin, *International Agricultural Engineering Journal* **26**, 193 (2017).
- [22] D. Du, B. Wang, J. Wang, F. Yao, and X. Hong, *Postharvest Biology and Technology* **152**, 36 (2019).
- [23] N. Sakurai, T. Takashima, H. Akimoto, and J. Blahovec, *J. Texture Studies* **52**, 480 (2021).
- [24] P. J. Jackson and F. R. Harker, *New Zealand Journal of Crop and Horticultural Science* **25**, 185 (1997).
- [25] T. Yoshida, Y. Tasaka, H. J. Park, Y. Murai, H. Teramura, and S. Koseki, *J. Visualization* **21**, 253 (2018).
- [26] B. Diezma-Iglesias, M. Ruiz-Altisent, and P. Barreiro, *Biosystems Engineering* **88**, 221 (2004).
- [27] M. Kadowaki, . Nagashima, H. Akimoto, and N. Sakurai, *Journal of the Japanese Society for Horticultural Science* , 327.
- [28] T. Kawai, F. Matsumori, H. Akimoto, N. Sakurai, K. Hirano, R. Nakano, and F. Fukuda, *Horticulture Journal* **87**, 499 (2018).
- [29] New Zealand Institute for Plant and Food Research Limited, *FreshFacts*, Tech. Rep. (2020).
- [30] A. Berardinelli, E. Iaccheri, L. Franceschelli, M. Tartagni, and L. Ragni, *IEEE Journal on Emerging and Selected Topics in Circuits and Systems* **11**, 515 (2021).
- [31] A. R. Ferguson, in *Horticultural Reviews*, 6, edited by J. Janick (1984) p. 1–64.
- [32] C. T. Nnodim, A. M. R. Fath El Bab, B. W. Ikua, and D. N. Sila, *Int. J. Mech. Mech. Eng.* **19**, 1 (2019).
- [33] J. L. Johnson, H. tom Wörden, and K. van Wijk, *Journal of Laboratory Automation* **20**, 10 (2015).
- [34] H. P. Crotwell, T. J. Owens, and J. Ritsema, *Seis. Res. Lett.* **70**, 154 (1999).
- [35] S. Stein and M. Wyssession, *An Introduction to Seismology, Earthquakes, and Earth Structure* (John Wiley & Sons, 2009).
- [36] N. Jiménez, R. Picó, F. Camarena, J. Redondo, and B. Roig, *Postharvest Biology and Technology* **67**, 130 (2012).
- [37] B. Pourkhak, S. A. M., M. Sadeghi, and A. Hemmat, *Measurement: Journal of the International Measurement Confederation* **101**, 157 (2017).
- [38] A. Mizrach, *Postharvest Biology and Technology* **48**, 315 (2008).
- [39] Y. Cheng and C. G. Haugh, *Transactions of the American Society of Agricultural Engineers* **37**, 217 (1994).
- [40] R. C. Clark and V. N. Rao, *J. Food Science* **42**, 1478 (1977).
- [41] J. Nicolas, M. Buret, F. Duprat, M. Nicolas, C. Rothan, and P. Moras, *Acta Horticulturae* **194**, 261 (1986).
- [42] P. Varela, A. Salvador, and S. Fiszman, *Journal of Food Engineering* **78**, 622 (2007).
- [43] N. Hosoya, M. Mishima, I. Kajiwara, and S. Maeda, *Postharvest Biol. Technol.* **128**, 11 (2017).